

Synthesis of Volatile, Reactive Coinage Metal 5,5-Bicyclic Amidinates with Enhanced Thermal Stability for Chemical Vapor Deposition

Liuchuan Tong, Luke M. Davis, Xian Gong, Jun Feng, Eugene S. Beh, and Roy G. Gordon

Department of Chemistry and Chemical Biology, Harvard University, Cambridge, MA 02138

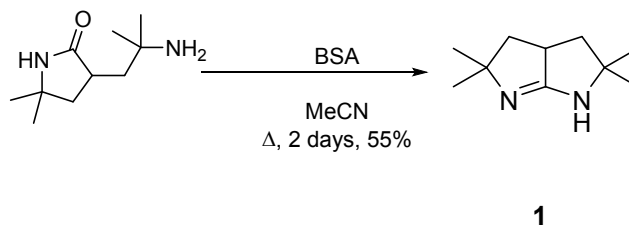
Email: gordon@chemistry.harvard.edu

SUPPORTING INFORMATION

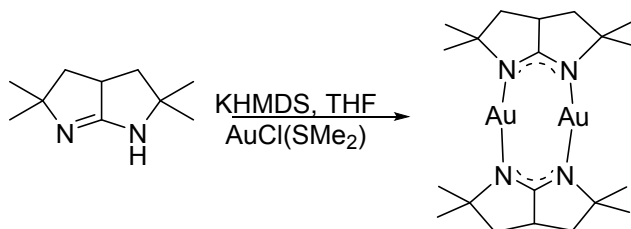
General information: ^1H NMR and ^{13}C NMR spectra were recorded on Varian Unity INOVA 500 spectrometers at 11.7 T in the Laukien-Purcell Instrumentation Center Magnetic Resonance Lab at Harvard University. NMR spectra were recorded in solutions of deuterated chloroform (CDCl_3) with the residual chloroform (7.24 ppm for ^1H NMR and 77.23 ppm for ^{13}C NMR) taken as the internal standard, or deuterated benzene (C_6D_6) with residual benzene (7.16 ppm for ^1H NMR and 128.39 ppm for ^{13}C NMR) taken as the internal standard, and were reported in parts per million (ppm). Mass spectra were recorded at the Harvard University mass spectrometry facility on a Bruker microTOF-QII instrument using a direct injection method with 0.1% formic acid, 50% water in acetonitrile as the mobile phase. Elemental analyses were performed by the University of Illinois at Urbana-Champaign Microanalysis lab. X-ray crystallographic data were collected at the Harvard University X-Ray Facility on a Bruker APEX DUO single crystal diffractometer. All reactions sensitive to moisture or oxygen were carried out in oven dried or flame dried and nitrogen-charged glassware, or in an argon-filled glovebox. Anhydrous solvents were saturated with nitrogen and dried with 4A molecular sieves purchased from Sigma-Aldrich. All other solvents and reagents were used as received from commercial suppliers without prior purification unless otherwise specified. The purity and identity of all new organic compounds was determined by NMR and mass spectrometry. The metal-containing compounds reported in this paper were also characterized by elemental analysis.

The compounds 3-(2-amino-2-methylpropyl)-5,5-dimethylpyrrolidin-2-one and copper(I) 2,2,5,5-tetramethyl-1,2,3,3a,4,5-hexahydropyrrolo[2,3-b]pyrrolide (compound **2**) were prepared by the previously reported methods.¹ 2,2,5,5-tetramethyl-1,2,3,3a,4,5-hexahydropyrrolo[2,3-b]pyrrole, **1**, was prepared by modification of the literature route,¹ as described below.

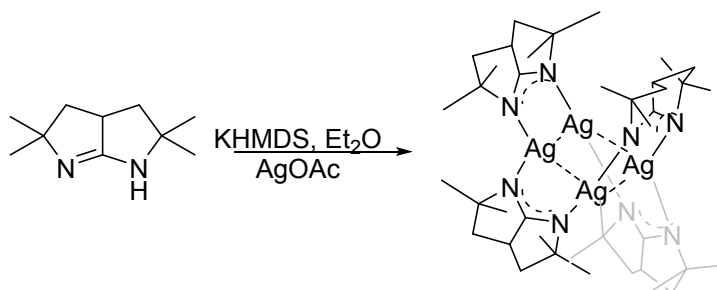
Synthesis and characterization



2,2,5,5-tetramethyl-1,2,3,3a,4,5-hexahydropyrrolo[2,3-b]pyrrole, compound 1. 3-(2-amino-2-methylpropyl)-5,5-dimethylpyrrolidin-2-one¹ (15 g, 81.4 mmol) was dissolved in 200 mL of acetonitrile. To the solution was added *N,O*-bis(trimethylsilyl)acetamide (BSA, 33.5 g, 160.0 mmol) over 3 hours. The solution was refluxed for 2 days, during which the progress of the reaction was monitored by NMR and more BSA was added if the NMR spectra indicated incomplete reaction (Scheme S_a). Once the reaction was complete, the solution was concentrated *in vacuo* and the resulting oil was dissolved in 200 mL of 3.0 M HCl and washed with CH₂Cl₂ (3 × 100 mL), then ice was added and **1** was precipitated by slowly adding 125 mL of cold 5.0 M NaOH. The suspension was then extracted with CH₂Cl₂ (4 × 100 mL), and the extracts were combined, dried over anhydrous sodium sulfate, and evaporated to afford crude **1** as a pale-yellow waxy solid. Oily impurities were collected by sublimation at 45 °C at 50 mTorr for 2 hours and discarded. Further sublimation of the remaining solid overnight at 70 °C at 50 mTorr gave pure, anhydrous **1** (7.4 g, 55%) as a white solid suitable for the synthesis of metal-containing CVD precursors, mp. 182-183 °C. ¹H NMR (500 MHz, C₆D₆) δ 9.20-8.45 (bs, 1H), 3.22-3.14 (m, 1H), 1.73-1.66 (m, 2H), 1.33 (s, 6H), 1.29-1.23 (m, 2H), 1.17 (s, 6H); ¹³C NMR (125 MHz, C₆D₆) δ 174.9, 69.8, 46.2, 45.3, 31.5, 29.1.



Dimeric gold(I) 2,2,5,5-tetramethyl-1,2,3,3a,4,5-hexahydropyrrolo[2,3-b]pyrrolide, 3. (100 mg, 0.601 mmol) of **1** was suspended in 100 mL of anhydrous THF. Potassium bis(trimethylsilyl)amide (126 mg, 0.633 mmol) was added, at which point all solids quickly dissolved. After stirring for 1 hour, chloro(dimethylsulfide)gold(I) (195 mg, 0.662 mmol) was added as a solid and the reaction mixture was allowed to stir overnight. The reaction mixture was filtered through a Celite pad, and the solvent removed under reduced pressure to afford a white solid that was rapidly washed with 10 mL of cold 1:1 THF:pentane to afford a mixture of diastereomers of **3** (110 mg, 51 %) as a slightly off-white solid. Recrystallization by vapor diffusion of hexanes into a dichloromethane solution of **3** provided white crystals suitable for single-crystal X-ray diffraction. The recrystallized material may be further purified by vacuum sublimation if so desired (180 °C, 30 mTorr). **Elemental Analysis** calcd. for C₂₀H₃₄Au₂N₄: C 33.2%, H 4.73 %, N 7.73 %; found C 33.1%, H 4.56 %, N 7.68%; ¹H NMR (500 MHz, C₆D₆) δ 3.15-3.08 (m, 2H), 1.56-1.53 (m, 4H), 1.24 (s, 6H), 1.23 (s, 6H), 1.23-1.19 (m, 4H), 1.04 (s, 6H), 1.02 (s, 6H). Mixture of two diastereomers of ratio ca. 43:57, based on integration of the methyl peak areas.

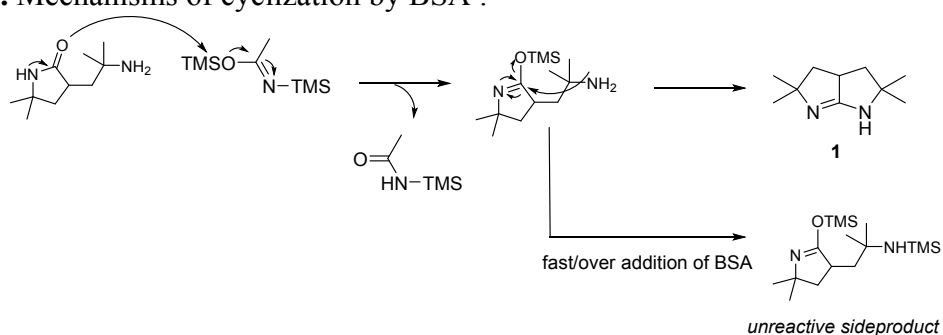


Tetrameric silver(I) 2,2,5,5-tetramethyl-1,2,3,3a,4,5-hexahydropyrrolo[2,3-b]pyrrolide, 4. (100 mg, 0.601 mmol) of **1** was suspended in 50 mL of anhydrous Et₂O. Potassium bis(trimethylsilyl)amide (126 mg, 0.633 mmol) was added, at which point all solids quickly dissolved. After stirring for 1 hour, silver(I) acetate (100 mg, 0.662 mmol) was added as a solid and the reaction mixture was allowed to stir overnight. The reaction mixture was filtered through a Celite pad and the solvent removed under reduced pressure to give an off-white solid. This solid was thoroughly stirred with 500 mL of pentane and filtered again through Celite. Evaporation of the pentane from the filtrate yielded crude **4** (65 mg, 40 %) as a slightly off-white solid. Recrystallization by vapor diffusion of hexanes into a dichloromethane solution of **4** afforded white crystals suitable for single-crystal X-ray diffraction. The recrystallized material may be further purified by vacuum sublimation if so desired (170 °C, 30 mTorr). **Elemental Analysis** calcd. for C₄₀H₆₈Ag₄N₈: C 44.0 %, H 6.27 %, N 10.3 %; found C 44.4%, H 6.22%, N 9.95%.

Notes on ligand synthesis.

The key step to the ligand synthesis requires that *N,O*-bis(trimethylsilyl)acetamide (BSA) be introduced to the reaction very slowly, with the reaction progress carefully monitored by NMR to avoid double trimethylsilylation which results in an unreactive intermediate (Scheme S_α).

Scheme S_α. Mechanisms of cyclization by BSA .



During the synthesis of the copper complex **2** by the literature route,¹ we found an interesting phenomenon. Despite the copper(I) complex being stable in air, the ESI-TOF MS detection of the compound dissolved in benzene/MeCN showed peaks at m/z ratios of 167 and 395, which correspond to the free ligand and mono-demetalated **2**; no parent ion ($m/z = 457$) was observed (Figure S1). This result showed that these metal complexes can be labile in MS conditions, in positive ion mode and with formic acid in the mobile phase. Although not quantitative, this signal provides a fast and definitive method of determining the success of the synthesis, which proved to be convenient in the silver and gold precursor syntheses. Similar MS fragmentation and oligomerization patterns have been reported previously for silver(I) amidinates.²

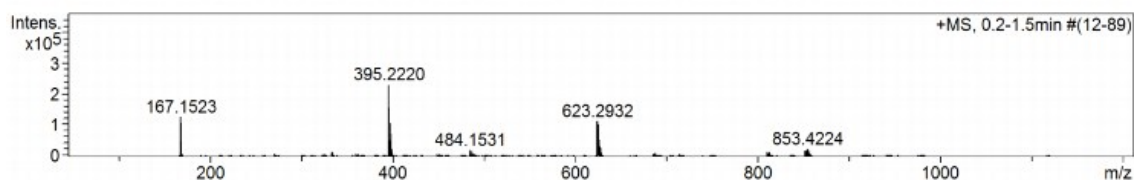


Figure S1. Mass-spectrometry data showing the existence of free ligand ($m/z = 167$), mono-demetalated **2** ($m/z = 395$), and higher clusters of copper ions and ligands generated by the ionization process.

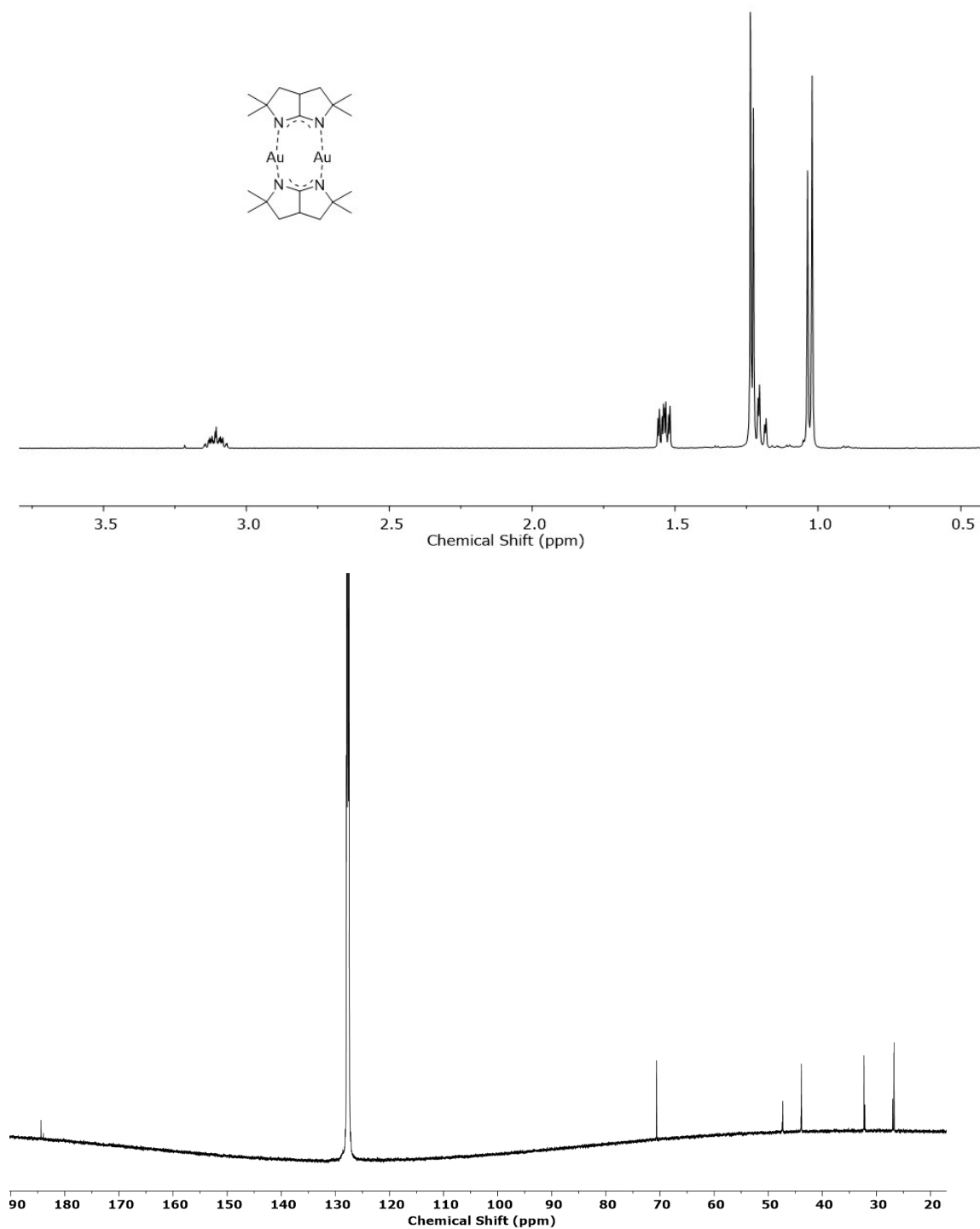


Figure S2. ^1H NMR (top) and ^{13}C NMR (bottom) spectrum of **3**. The doublets indicate the existence of two diastereomers.

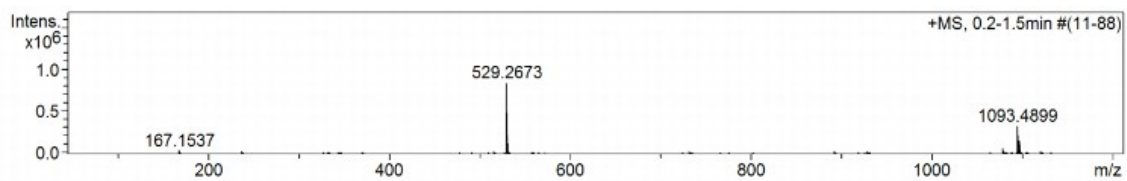


Figure S3. Mass-spectrometry data showing the existence of free ligand ($m/z = 167$), mono-demetalated, dimeric **3** ($m/z = 529$), and a higher cluster of gold ions and ligands generated by the ionization process.

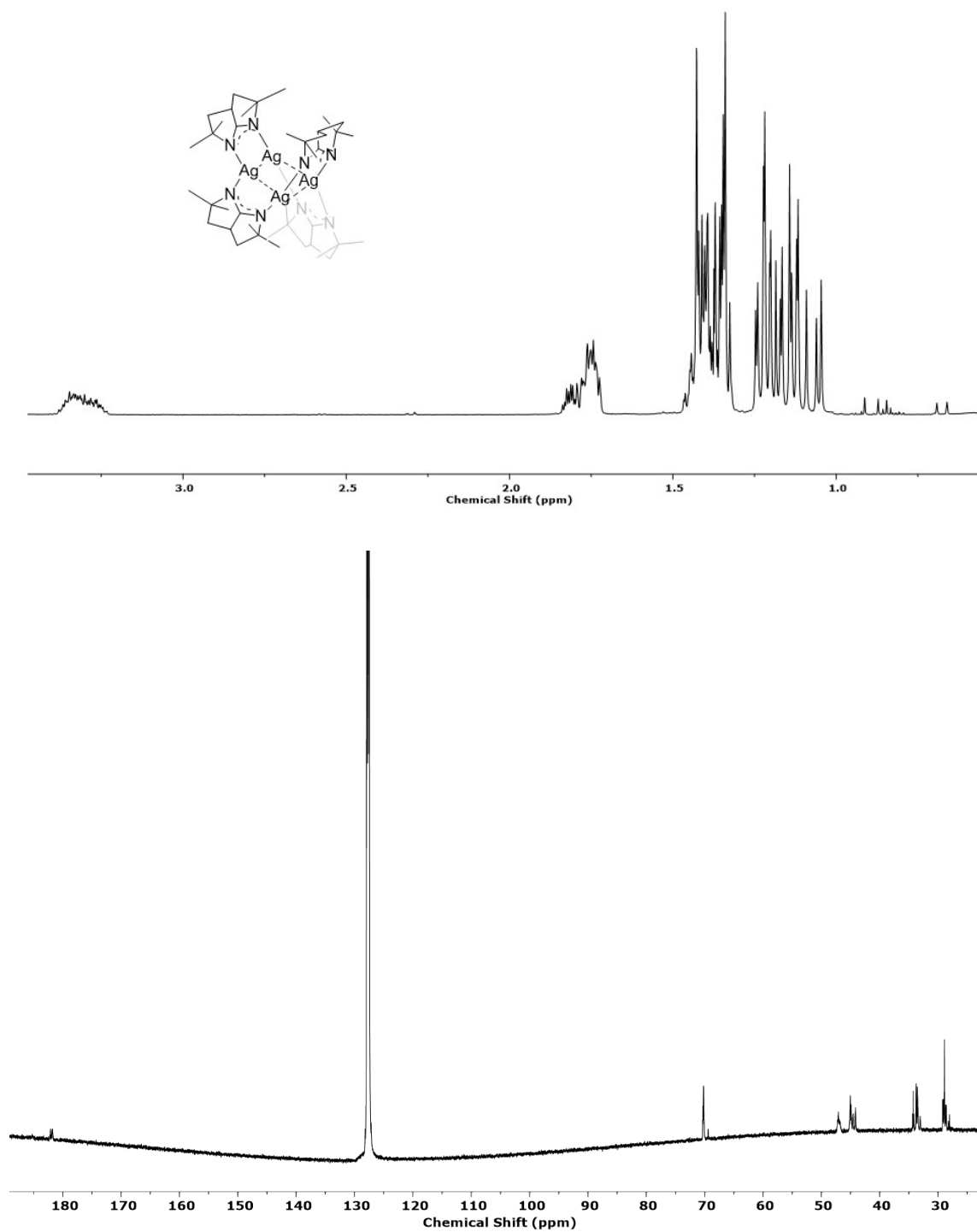


Figure S4. ^1H NMR (top) and ^{13}C NMR (bottom) spectrum of **4**.

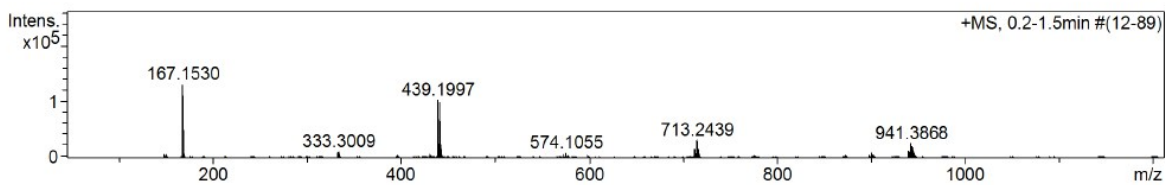


Figure S5. Mass-spectrometry data showing the existence of free ligand ($m/z = 167$), mono-demetalated, dimeric **4** ($m/z = 439$), and higher clusters of silver ions and ligands generated by the ionization process.

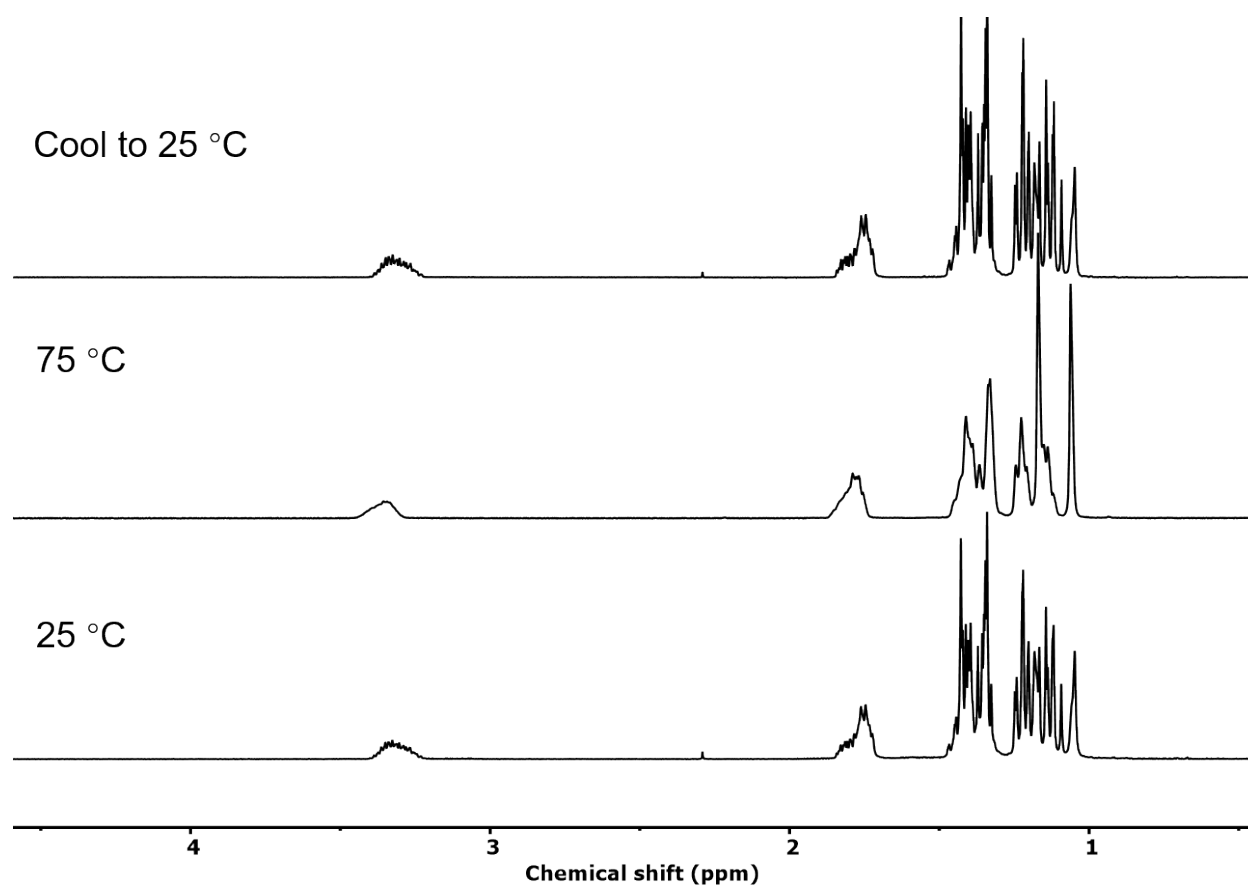


Figure S6. Variable-temperature ^1H NMR of **4** in C_6D_6 showing a reversible simplification of the NMR spectrum, indicating the reversible transition of the tetrameric silver complex to lower order clusters.

Crystallographic Studies.³ Single crystals of Au₂(N₂C₁₀H₁₇)₂ (**3**) and Ag₄(N₂C₁₀H₁₇)₄ (**4**) were grown by vapor diffusion of hexane into dichloromethane at 25 °C. The crystals were mounted on a MiTeGen MicroMount™ with Paratone-N oil, and immediately cooled to -173 °C in a cold nitrogen gas stream on the diffractometer, a Bruker three-circle platform goniometer equipped with an Apex II CCD and an Oxford cryostream cooling device. Standard peak search and indexing procedures, followed by least squares refinement, yielded the cell dimensions given in Table S1. Data were collected with an area detector by using the measurement parameters listed in Table S1. The measured intensities were reduced to structure factor amplitudes and their esd's by correction for background, scan speed, Lorentz and polarization effects. No corrections for crystal decay were necessary. Face-indexed absorption corrections were applied, with the absorption coefficient and maximum and minimum transmission factors listed in Table S1. Systematically absent reflections were deleted, and symmetry equivalent reflections were averaged to yield the set of unique data. The remaining 2572 unique data for **3** and 2070 unique data for **4** were used in the least-squares refinements. In the final cycle of least squares refinement, independent anisotropic displacement parameters were refined for the non-hydrogen atoms. All hydrogen atoms were fixed in "idealized" positions with C-H = 0.98 Å (methyl), 0.99 Å (methylene), or 1.00 Å (methine). Methyl groups were allowed to rotate about the C-C axis to find the best least-squares hydrogen atom positions. Isotropic displacement parameters for methyl hydrogen atoms were set to 1.5 times Ueq of the attached carbon, and for methylene and methine groups to 1.2 times Ueq. Successful convergence was indicated by the maximum shift/error of 0.001 for the last cycle. A final analysis of variance between observed and calculated structure factors showed no apparent errors.

3: The orthorhombic lattice and systematic absences for $0kl$ ($k \neq 2n$), $h0l$ ($l \neq 2n$), and $hk0$ ($h \neq 2n$) were consistent only with space group *Pbca*, the selection of which was supported by the success of the subsequent refinement. The structure was solved by direct methods (SHELXTL); the correct positions for the gold atoms were deduced from the initial E-map. Subsequent least-squares refinement and difference Fourier calculations revealed the locations of the nitrogen and carbon atoms. The quantity minimized in the least-squares program was $\Sigma w(F_o^2 - F_c^2)^2$, where $w = \{[\sigma(F_o^2)]^2 + (0.0429 P)^2 + 2.50 P\}^{-1}$ and $P = (F_o^2 + 2F_c^2)/3$. An isotropic extinction parameter was refined to a final value of $x = 5.7(7) \times 10^{-7}$ where F_c is multiplied by $k[1 + xF_c^2\lambda^3/\sin 2\theta]^{-1/4}$ and k is the overall scale factor. The largest peak and hole in the final Fourier difference map (2.78 and -1.31 eÅ⁻³) were located, respectively, 0.79 Å and 0.95 Å from Au1, and likely result from minor errors in the absorption correction.

4: The orthorhombic lattice and systematic absences for hkl ($h + k$ or $k + l$ or $l + h \neq 2n$), $0kl$ ($k + l \neq 4n$), $h0l$ ($h + l \neq 4n$), and $hk0$ ($h + k \neq 4n$) were consistent only with space group *Fddd*, the selection of which was supported by the success of the subsequent refinement. The structure was solved by direct methods (SHELXTL); the correct positions for the silver and nitrogen atoms were deduced from the initial E-map. Subsequent least-squares refinement and difference Fourier calculations revealed the locations of the carbon atoms, including the disordered ones. The quantity minimized in the least-squares program was $\Sigma w(F_o^2 - F_c^2)^2$, where $w = \{[\sigma(F_o^2)]^2 + (0.0140 P)^2\}^{-1}$ and $P = (F_o^2 + 2F_c^2)/3$. The carbon atoms not attached to nitrogen atoms were best modeled as disordered over two positions, and the site occupancy factors (SOFs) for the alternative locations were restrained to sum to unity. The SOF of the major component refined to 0.752. No extinction parameter was necessary. The largest peak and hole in the final Fourier difference map (0.40 and -0.27 eÅ⁻³) were located, respectively, 1.13 Å from H3A and 0.57 Å from H7B1.

Table S1. Crystallographic data for compounds **3** and **4**.

	3	4
formula	Au ₂ N ₄ C ₂₀ H ₃₄	Ag ₄ N ₈ C ₄₀ H ₆₈
formula weight	724.45	1092.49
<i>T</i> (K)	100(2)	100(2)
λ (Å)	0.71073	0.71073
crystal system	orthorhombic	orthorhombic
space group	<i>Pbca</i>	<i>Fddd</i>
<i>a</i> (Å)	11.691(1)	11.305(2)
<i>b</i> (Å)	10.832(1)	23.157(3)
<i>c</i> (Å)	17.634(1)	33.145(5)
<i>V</i> (Å ³)	2233(1)	8677(2)
<i>Z</i> , ρ_{calc} (g cm ⁻³)	4, 2.155	8, 1.673
μ (mm ⁻¹)	13.134	1.816
<i>F</i> (000)	1360	4416
crystal size (mm)	0.17×0.17×0.09	0.12×0.10×0.05
θ range (°)	2.31 – 27.54	2.10 – 25.68
<i>R</i> (int)	0.0712	0.0644
absorption correction	face-indexed	face-indexed
max., min. transmission factors	0.878, 0.756	0.922, 0.862
data / restraints / parameters	2572 / 0 / 123	2070 / 229 / 191
GOF on <i>F</i> ²	1.069	0.921
<i>R</i> ₁ [<i>I</i> > 2 σ (<i>I</i>)]	0.0240	0.0201
<i>wR</i> ₂ (all data)	0.0669	0.0360
max., min. $\Delta\rho_{\text{elect}}$ (e Å ⁻³)	2.78, -1.31	0.40, -0.27

Table S2. Selected distances (Å) and angles (°) for compound **3**.

Au(1)-Au(1A)	2.855(1)	C(3)-C(4)	1.554(5)	N(1A)-C(1)-N(2)	132.5(4)
Au(1)-N(1)	2.013(3)	C(10)-C(7)	1.547(6)	N(1A)-C(1)-C(2A)	113.6(3)
Au(1)-N(2)	2.013(3)	C(4)-C(5)	1.534(6)	N(2)-C(1)-C(2A)	113.9(3)
N(1)-C(1A)	1.324(5)	C(4)-C(6)	1.510(6)	C(1A)-N(1)-C(4)	108.9(3)
N(1)-C(4)	1.492(5)	C(7)-C(8)	1.503(6)	C(1A)-N(1)-Au(1)	119.4(3)
N(2)-C(1)	1.314(5)	C(7)-C(9)	1.536(6)	C(4)-N(1)-Au(1)	131.7(3)
N(2)-C(7)	1.499(4)			C(1)-N(2)-C(7)	109.0(3)
C(1)-C(2)	1.510(5)	N(1)-Au(1)-N(2)	167.4(1)	C(1)-N(2)-Au(1)	120.4(3)
C(2)-C(3)	1.495(6)	N(1)-Au(1)-Au(1A)	83.4(1)	C(7)-N(2)-Au(1)	130.6(3)
C(2)-C(10)	1.487(6)	N(2)-Au(1)-Au(1A)	84.0(1)		

Table S3. Selected distances (Å) and angles (°) for compound **4**.

Ag(1)-Ag(1A)	3.096(1)	C(1)-C(4)	1.520(4)	C(1)-C(4B)	1.514(8)
Ag(1)-Ag(2)	3.296(1)	C(2)-C(7)	1.510(4)	C(2)-C(7B)	1.533(8)
Ag(1)-Ag(2A)	3.296(1)	C(2)-C(8)	1.529(4)	C(2)-C(8B)	1.522(7)
Ag(2)-Ag(1A)	3.296(1)	C(2)-C(3)	1.561(4)	C(2)-C(3B)	1.541(7)
Ag(2)-Ag(2A)	5.820(2)	C(3)-C(4)	1.522(5)	C(3B)-C(4B)	1.508(8)
Ag(1)-N(1)	2.094(2)	C(4)-C(5)	1.520(5)	C(4B)-C(5B)	1.507(8)
Ag(2)-N(2)	2.054(2)	C(5)-C(6)	1.555(4)	C(5B)-C(6)	1.555(7)
N(1)-C(1)	1.319(3)	C(6)-C(9)	1.525(4)	C(6)-C(9B)	1.518(8)
N(2)-C(1)	1.305(3)	C(6)-C(10)	1.522(4)	C(6)-C(10B)	1.514(7)
N(1)-C(2)	1.505(3)				
N(2)-C(6)	1.496(3)			N(1)-Ag(1)-N(1A)	165.5(1)
		N(1)-C(1)-N(2)	131.9(2)	N(2)-Ag(2)-N(2A)	178.0(1)
C(1)-N(1)-Ag(1)	129.4(2)	C(1)-N(2)-Ag(2)	123.5(2)	Ag(1)-Ag(2)-Ag(1A)	56.02(1)
C(2)-N(1)-Ag(1)	122.2(2)	C(6)-N(2)-Ag(2)	127.6(2)	Ag(2)-Ag(1)-Ag(1A)	61.99(1)
C(1)-N(1)-C(2)	107.9(2)	C(1)-N(2)-C(6)	108.8(2)	Ag(2)-Ag(1)-Ag(2A)	124.0(2)

Table S4. Complete list of angles (°) for compound **3**.

Atom	Atom	Atom	Angle	Atom	Atom	Atom	Angle
N2	Au1	N1	167.44(13)	N1	C4	C3	103.1(3)
N2	Au1	Au1 ¹	83.40(9)	C6	C4	C3	112.9(4)
N1	Au1	Au1 ¹	84.04(10)	C5	C4	C3	111.5(4)
C1 ¹	N1	C4	108.9(3)	N2	C7	C8	109.6(3)
C1 ¹	N1	Au1	119.4(3)	N2	C7	C9	110.0(3)
C4	N1	Au1	131.7(3)	C8	C7	C9	109.9(4)
C1	N2	C7	109.0(3)	N2	C7	C10 ¹	102.7(3)
C1	N2	Au1	120.4(3)	C8	C7	C10 ¹	112.7(4)
C7	N2	Au1	130.6(3)	C9	C7	C10 ¹	111.7(4)
N2	C1	N1 ¹	132.5(4)	C2	C3	C4	105.1(3)
N2	C1	C2 ¹	113.6(3)	C10	C2	C3	130.9(4)
N1 ¹	C1	C2 ¹	113.9(3)	C10	C2	C1 ¹	100.6(3)
N1	C4	C6	109.9(3)	C3	C2	C1 ¹	100.7(3)
N1	C4	C5	109.0(3)	C2	C10	C7 ¹	105.1(4)
C6	C4	C5	110.3(4)				

Table S5. Complete angles (°) for compound **4**.

¹: 9/4-X,+Y,1/4-Z; ²: 9/4-X,5/4-Y,+Z

Atom	Atom	Atom	Angle	Atom	Atom	Atom	Angle
N1 ¹	Ag1	N1	165.47(12)	C8B	C2	C3B	115.8(6)
N1 ¹	Ag1	Ag1 ²	97.26(6)	C8	C2	C3B	86.3(5)
N1	Ag1	Ag1 ²	97.26(6)	C7B	C2	C3B	108.8(8)
N1 ¹	Ag1	Ag2	112.71(6)	N1	C2	C3	102.5(2)
N1	Ag1	Ag2	74.50(6)	C7	C2	C3	112.7(3)
Ag1 ²	Ag1	Ag2	61.988(7)	C8B	C2	C3	138.0(5)
N1 ¹	Ag1	Ag2 ¹	74.50(6)	C8	C2	C3	111.5(3)
N1	Ag1	Ag2 ¹	112.71(6)	C7B	C2	C3	86.4(6)
Ag1 ²	Ag1	Ag2 ¹	61.986(7)	C3B	C2	C3	26.3(5)
Ag2	Ag1	Ag2 ¹	123.974(13)	C4	C3	C2	103.8(3)
N2 ²	Ag2	N2	177.98(12)	C1	C4	C5	99.8(3)
N2 ²	Ag2	Ag1 ²	80.37(6)	C1	C4	C3	98.5(3)
N2	Ag2	Ag1 ²	101.44(6)	C5	C4	C3	125.6(5)
N2 ²	Ag2	Ag1	101.44(6)	C5B	C4B	C3B	128.3(13)
N2	Ag2	Ag1	80.37(6)	C5B	C4B	C1	96.2(8)
Ag1 ²	Ag2	Ag1	56.024(13)	C3B	C4B	C1	101.0(8)

C1	N1	C2	107.9(2)	C4	C5	C6	102.0(3)
C1	N1	Ag1	129.37(17)	N2	C6	C10B	111.0(9)
C2	N1	Ag1	122.23(16)	N2	C6	C9B	105.3(7)
C1	N2	C6	108.8(2)	C10B	C6	C9B	113.3(10)
C1	N2	Ag2	123.51(17)	N2	C6	C10	108.7(3)
C6	N2	Ag2	127.57(17)	C10B	C6	C10	25.0(6)
N2	C1	N1	131.9(2)	C9B	C6	C10	91.0(8)
N2	C1	C4B	114.6(5)	N2	C6	C9	113.3(3)
N1	C1	C4B	111.4(4)	C10B	C6	C9	124.8(8)
N2	C1	C4	113.1(3)	C9B	C6	C9	23.3(6)
N1	C1	C4	114.9(3)	C10	C6	C9	107.7(4)
C4B	C1	C4	17.6(7)	N2	C6	C5B	100.9(5)
N1	C2	C7	110.0(3)	C10B	C6	C5B	113.5(7)
N1	C2	C8B	108.8(5)	C9B	C6	C5B	111.9(8)
C7	C2	C8B	82.2(6)	C10	C6	C5B	136.1(6)
N1	C2	C8	109.1(3)	C9	C6	C5B	88.7(5)
C7	C2	C8	110.7(3)	N2	C6	C5	103.5(2)
C8B	C2	C8	31.5(5)	C10B	C6	C5	87.2(6)
N1	C2	C7B	112.9(7)	C9B	C6	C5	134.9(7)
C7	C2	C7B	26.9(6)	C10	C6	C5	111.6(3)
C8B	C2	C7B	105.7(8)	C9	C6	C5	112.1(3)
C8	C2	C7B	129.0(7)	C5B	C6	C5	27.8(4)
N1	C2	C3B	105.0(5)	C4B	C3B	C2	101.5(7)
C7	C2	C3B	132.4(6)	C4B	C5B	C6	105.2(7)

Table S6. Distances and angles of the interactions between the gold(I) centers of one molecule of **3** and the methyl groups of its neighbor.

Au \cdots H-C Interaction	d(Au \cdots H), Å	d(Au \cdots C), Å	\angle (Au-H-C), °
Au(1E) \cdots H-C(10B)	2.932(2)	3.910(6)	169.6(2)
Au(1F) \cdots H-C(9A)	2.968(2)	3.895(6)	158.4(3)
Au(1F) \cdots H-C(9A)	3.202(2)	4.072(5)	149.0(3)

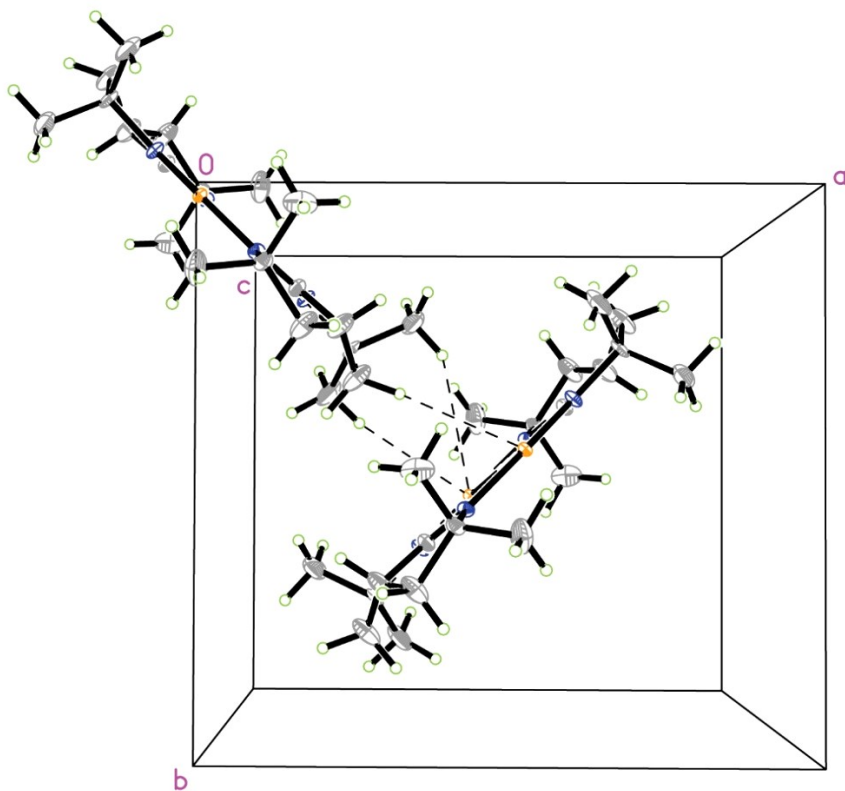


Figure S7. Partial packing diagram of **3**, showing the relation between nearest neighbors. Truncated versions of these molecules are shown from a different angle in the main text.

Comparison of structures to literature compounds.

In **3**, the Au-N distances of 2.013(3) Å are on the shorter end of typical; the reported range is 2.025(9)-2.085(7) Å in digold(I)⁴⁻⁷ amidinates and 2.000(4)-2.057(11) Å in tetragold(I) complexes.⁸⁻¹¹ The Au⋯Au distance is 2.855(1) Å, more similar to the 2.902(1)-3.049(1) Å found in tetragold(I) amidinates⁸⁻¹⁰ than the 2.644(2)-2.711(3) Å reported for other digold(I) amidinates.⁴⁻⁷ In **3**, the combination of the short Au-N distances and the N-C-N angle leads to bent N-Au-N angles of 167.4(1)°. Gold(I) amidinate and guanidinate dimers typically have N-Au-N angles of 167.7(3)°-170.8(4)°,⁴⁻⁷ however, so this effect is not strong.

In **4**, the N-Ag-N angles are asymmetric, with one angle approaching the preferred linear coordination geometry of silver(I), 178.0(1)°, and the other substantially contracted to 165.5(1)°. This asymmetry is not unusual, with N-Ag-N angles varying as much as 156.3(2)° to 178.4(2)° within a single tetranuclear molecule.^{2, 12} Although the Ag⋯Ag distances of 3.296(2) Å along the sides of **4** are unusually long, the cross distance of 3.096(2) Å (Ag(1)⋯Ag(1A)) falls into the previously observed range of 3.077(1)-3.220(1) Å.^{2, 12} Disilver(I) and trisilver(I) complexes typically have shorter Ag⋯Ag distances also, in the range of 2.645(1)-2.754(1) Å^{4, 13-15} and 2.955(1)- 3.217(1) Å,^{6, 7, 13} respectively.

Regarding the disorder in **4**, the high symmetry of the site on which the molecule sits in the unit cell prevents us from determining the distribution of this conformation across molecules in the lattice (e.g., whether, say, ¼ of the molecules have every ligand inverted, or every molecule has ¼ of the ligands inverted).

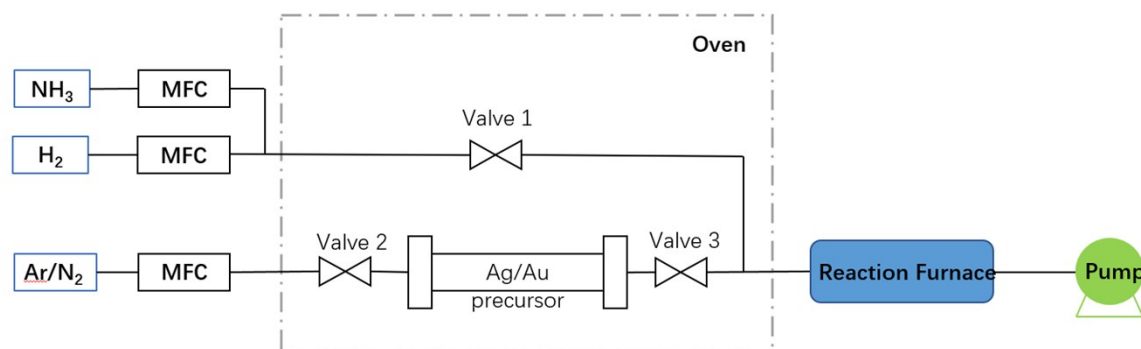
Thermogravimetric Analysis (TGA). TGA experiments were performed with a TA Instruments Model Q50 system in a glovebox. N₂ was used as the flow gas (balance gas: 40 mL/min, sample gas: 40.0 mL/min). Aluminum sample pans (100 μL, TA Instruments Cat. #: 952323.902) with diameter 1 cm were used for this experiment; a new pan was used for each experiment.

Ramp TGA experiments: ca. 10 mg of **2**, **3**, and **4** were used for ramp TGA with a heating rate of 10 °C/min.

Isothermal TGA experiments: These experiments were performed to obtain the temperature dependence of the evaporation rate. In a typical experiment, a sample pan was loaded with ca. 10 mg of sample material, and then heated at 10 °C/min to the first isotherm temperature. After the temperature stabilized, it was maintained for 11 minutes to collect isothermal weight loss data at that temperature. The temperature was then raised to the next isotherm temperature following the same protocol. The isotherm temperatures were 170, 180, 190, 200, 210, 220, 230 °C. A plot of ln(rate constant of sublimation) vs the reciprocal of temperature in Kelvin yields the slope as the activation energy for sublimation according to the Arrhenius equation:

$$\ln(k) = \ln(A) - \frac{E_a}{RT}$$

CVD of gold and silver thin films



Scheme 1. Schematics of home-made CVD reactor

The CVD of gold and silver is conducted in a flow-through-type CVD reactor described in detail previously,¹⁶ the precursor delivery system of which is illustrated in Scheme 2. In detail, the molecular precursor **3** or **4** is stored in a tube-shape glass container with CF flange connectors at both ends. After being heated to ca. 160-180 °C, the precursor is delivered into the reaction chamber with a flow (100 sccm) of Ar or N₂ carrier gas. At the same time, continuous flow of purified H₂ gas is delivered into the reaction chamber to mix with the precursor, reducing the precursor to metal films. The reaction chamber is heated by a tube furnace and a built-in substrate heater. The substrate is heated to a slightly higher temperature (~10 °C) than the surrounding tube wall, so that the deposition mainly occurs on the substrates. We used thermal oxide silicon (300 nm of wet-oxidation SiO₂ on Si) coupons and glass slides as the substrates for depositions.

Characterization of gold and silver films

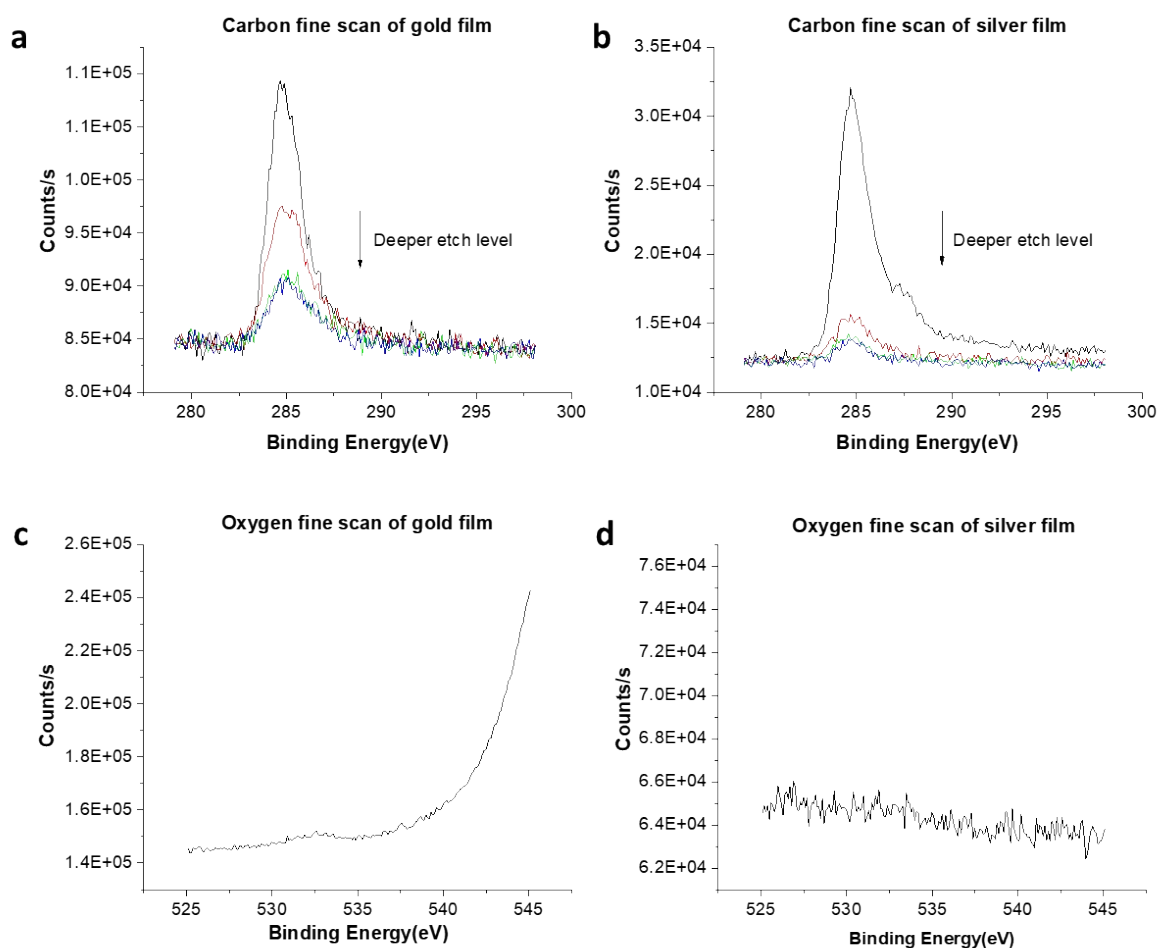


Figure S8. **a)** Carbon fine scans of a CVD gold film at several etch levels. **b)** Carbon fine scan of a CVD silver film at several etch levels. **c)** Oxygen fine scan of a CVD gold film at the deepest etch level. **d)** Oxygen fine scan of a CVD silver film at the deepest etch level.

XPS carbon fine scans demonstrate that carbon peaks of both gold and silver film decrease as etching levels go deeper. Atomic percentage of carbon was calculated based on the area of all peaks and XPS relative sensitivity factors.

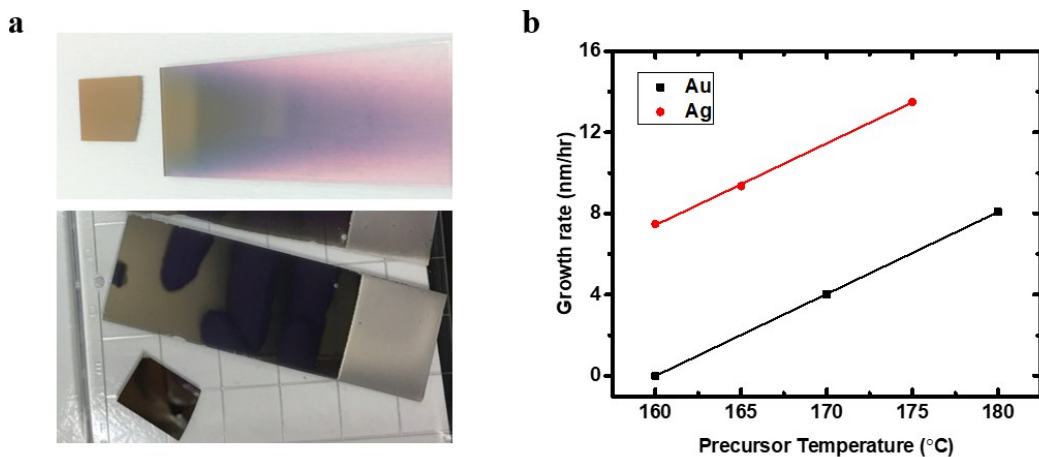


Figure S9. a) Photos of deposited gold film (top) and silver film (bottom). b) growth rate increases linearly with precursor temperature.

Table S7. Selected gold depositions with conditions and their corresponding growth and electrical properties.

Selected Gold Depositions Summary						
No.	Deposition Condition				Thickness (nm) / Growth Rate (nm/hrs)	Conductivity (Ω .nm)
	Bub T (°C)	Sub T (°C)	Gas	Time (hrs)		
Au 005	170	230/235	100 N ₂	13	No film	Not conductive
Au 006	170	230/235	100:100 H ₂ :N ₂	6.5	100.1 / 15.4	245.31
Au 008	185	200/208	100:100 H ₂ :N ₂	14	123.3 / 8.8	221.94
Au 009	185	200/209	100:100:100 H ₂ :N ₂ :NH ₃	15	53.35/3.56	250.75

Table S8. Selected silver depositions with conditions and their corresponding growth, elemental composition, and electrical properties.

Selected Silver Depositions Summary									
No.	Deposition Condition				Thickness (nm) / Growth Rate (nm/hrs)	XPS Composition (Deepest etching level)			Conductivity (Ω .nm)
	Bub T (°C)	Sub T (°C)	Gas	Time (hrs)		Ag	C	O	
Ag 002	160	200/209	100:100 H ₂ :N ₂	14	66 / 5.08	61.04	35.14	3.82	2224
Ag 010	170	229/232	100:100 H ₂ :Ar	18	168.33 / 9.35	83.5	16.5	0	1500
Ag 011	170	225/232	200:100 H ₂ :Ar	18	238.2 / 14.01	93.39	6.61	0	192.5
Ag 012	170	217/231	100 Ar	17	20 / 1.18	23.37	47.91	14.33	Not

References

1. E. S. Beh, L. Tong and R. G. Gordon, *Organometallics*, 2017, **36**, 1453-1456.
2. S. J. Archibald, N. W. Alcock, D. H. Busch and D. R. Whitcomb, *J. Cluster Sci.*, 2000, **11**, 261-283.
3. J. L. Brumaghim, J. G. Priepot and G. S. Girolami, *Organometallics*, 1999, **18**, 2139-2144.
4. D. Fenske, G. Baum, A. Zinn and K. Dehnicke, *Z. Naturforsch. B*, 1990, **45**, 1273-1278.
5. H. E. Abdou, A. A. Mohamed and J. John P. Fackler, *Inorg. Chem.*, 2005, **44**, 166-168.
6. T. J. J. Whitehorne, J. P. Coyle, A. Mahmood, W. H. Monillas, G. P. A. Yap and S. T. Barry, *Eur. J. Inorg. Chem.*, 2011, 3240-3247.
7. S. K. Adas, J. A. Ocana and S. D. Bunge, *Aust. J. Chem.*, 2014, **67**, 1021-1029.
8. E. Hartmann and J. Strähle, *Z. Naturforsch. B*, 1989, **44**, 1-4.
9. A. A. Mohamed, H. E. Abdou, M. D. Irwin, J. M. López-de-Luzuriaga and J. John P. Fackler, *J. Cluster Sci.*, 2003, **14**, 253-266.
10. H. E. Abdou, A. A. Mohamed, J. M. López-de-Luzuriaga and J. John P. Fackler, *J. Cluster Sci.*, 2004, **15**, 397-411.
11. A. A. Mohamed, A. P. Mayer, H. E. Abdou, M. D. Irwin, L. M. Pérez and J. John P. Fackler, *Inorg. Chem.*, 2007, **46**, 11165-11172.
12. M. D. Irwin, H. E. Abdou, A. A. Mohamed and J. John P. Fackler, *Chem. Commun.*, 2003, 2882-2883.
13. B. S. Lim, A. Rahtu, J.-S. Park and R. G. Gordon, *Inorg. Chem.*, 2003, **42**, 7951-7958.
14. A. C. Lane, M. V. Vollmer, C. H. Laber, D. Y. Melgarejo, G. M. Chiarella, J. John P. Fackler, X. Yang, G. A. Baker and J. R. Walensky, *Inorg. Chem.*, 2014, **53**, 11357-11366.
15. S. Wang, N. Harmgarth, P. Leibing and F. T. Edelmann, *Acta Cryst.*, 2016, **E72**, 1786-1790.
16. Y. Au, Y. Lin and R. G. Gordon, *J. Electrochem. Soc.*, 2011, **158**, D248-D253.